Atmos. Chem. Phys., 11, 8543–8554, 2011
www.atmos-chem-phys.net/11/8543/2011/
doi:10.5194/acp-11-8543-2011

Atmospheric Chemistry and Physics

A high spatial resolution retrieval of NO_2 column densities from OMI: method and evaluation

A. R. Russell[1], **A. E. Perring**[1,*,**], **L. C. Valin**[1], **E. J. Bucsela**[2], **E. C. Browne**[1], **K.-E. Min**[1], **P. J. Wooldridge**[1], **and R. C. Cohen**[1,3]

[1]Department of Chemistry, University of California Berkeley, Berkeley, CA, USA
[2]SRI International, Menlo Park, CA 94025, USA
[3]Department of Earth and Planetary Sciences, University of California Berkeley, Berkeley, CA, USA
[*]now at: Chemical Sciences Division, Earth Systems Research Laboratory, National Oceanic and Atmospheric Administration, Boulder, CO, USA
[**]now at: Cooperative Institute for Research in Environmental Sciences, University of Colorado Boulder, Boulder, CO, USA

Received: 17 March 2011 – Published in Atmos. Chem. Phys. Discuss.: 20 April 2011
Revised: 20 July 2011 – Accepted: 8 August 2011 – Published: 22 August 2011

Abstract. We present a new retrieval of tropospheric NO_2 vertical column density from the Ozone Monitoring Instrument (OMI) based on high spatial and temporal resolution terrain and profile inputs. We compare our NO_2 product, the Berkeley High-Resolution (BEHR) product, with operational retrievals and find that the operational retrievals are biased high (30 %) over remote areas and biased low (8 %) over urban regions. Additionally, we find non-negligible impacts on the retrieved NO_2 column for terrain pressure (±20 %), albedo (±40 %), and NO_2 vertical profile (−75 %–+10 %). We validate the operational and BEHR products using boundary layer aircraft observations from the Arctic Research of the Composition of the Troposphere from Aircraft and Satellites (ARCTAS-CA) field campaign which occurred in June 2008 in California. Results indicate that columns derived using our boundary layer extrapolation method show good agreement with satellite observations ($R^2 = 0.65$–0.83; $N = 68$) and provide a more robust validation of satellite-observed NO_2 column than those determined using full vertical spirals ($R^2 = 0.26$; $N = 5$) as in previous work. Agreement between aircraft observations and the BEHR product ($R^2 = 0.83$) is better than agreement with the operational products ($R^2 = 0.65$–0.72). We also show that agreement between satellite and aircraft observations can be further improved (e.g. BEHR: $R^2 = 0.91$) using cloud information from the Moderate Resolution Imaging Spectroradiometer (MODIS) instrument instead of the OMI cloud product. These results indicate that much of the variance in the operational products can be attributed to coarse resolution terrain pressure, albedo, and profile parameters implemented in the retrievals.

Correspondence to: R. C. Cohen
(rccohen@berkeley.edu)

1 Introduction

Nitrogen oxides ($NO_x \equiv NO + NO_2$) play a major role in determining atmospheric composition. NO_x affects the rate of tropospheric ozone production and influences the oxidative capacity of the atmosphere through regulation of OH, thereby acting as a feedback on its own chemical lifetime. Further, oxidation products of NO_x are contributors to atmospheric aerosol. Until recently, routine observation of NO_x was restricted to sparse surface networks concentrated in urban regions. The introduction of satellite remote-sensing instruments over the past decade, however, has provided global, routine observation of NO_2 leading to new insights into the spatial patterns of NO_x emissions and chemistry, and into the factors influencing NO_x sources. Satellite observations have provided exquisite evidence for spatial and temporal patterns in anthropogenic NO_x emissions (e.g. Kim et al., 2006, 2009; Martin et al., 2006; Mijling et al., 2009; Franke et al., 2009; Russell et al., 2010; Lin and McElroy, 2011; Valin et al., 2011), agricultural NO_x emissions (Bertram et al., 2005; Jaeglé et al., 2005; Hudman et al., 2010), lightning NO_x emissions (Beirle et al., 2004, 2006, 2009; Boersma et al., 2005; Martin et al., 2007; Bucsela et al., 2010), and fire NO_x emissions (Mebust et al., 2011).

Published by Copernicus Publications on behalf of the European Geosciences Union.

With a spatial footprint of $13 \times 24\,km^2$ at nadir, the Ozone Monitoring Instrument (OMI) has the highest spatial resolution of all the current space-based, NO_2-observing instruments. Operational retrieval of NO_2 vertical column density performed by the National Aeronautics and Space Administration Goddard Space Flight Center (NASA-GSFC) and the Netherlands Royal Meteorological Institute (KNMI) relies on coarsely resolved databases for terrain height, albedo, and NO_2 vertical profile shape. These inputs all have coarser spatial and temporal resolutions than the OMI observation. There is evidence that higher resolution albedo and surface pressure would improve the retrieval products (Schaub et al., 2007; Zhou et al., 2009; Hains et al., 2010; Heckel et al., 2011). There is also evidence that higher temporal resolution in the assumed profile will change the retrieval by as much as 74 % seasonally (Lamsal et al., 2010). However, a retrieval utilizing parameters that are all as spatially resolved as the OMI observation, as well as highly temporally resolved, has not been implemented and tested against in situ observations.

Here we develop a new retrieval of tropospheric NO_2 column, compare it to operational products, and finally, validate it with a robust in situ dataset from the California portion of the Arctic Research of the Composition of the Troposphere from Aircraft and Satellites (ARCTAS-CA) field campaign. Our new retrieval – hereafter referred to as the Berkeley High Resolution (BEHR) retrieval – uses much higher spatial and temporal resolution terrain and profile inputs than the operational retrievals. We examine aspects of the BEHR retrieval to show that it is an improvement over the low resolution products available, particularly in regions where terrain or albedo are varying on spatial scales comparable to the dimensions of the satellite pixel. We then evaluate the BEHR and operational retrievals using aircraft observations collected within the planetary boundary layer. We show that a large ensemble of observations collected in the boundary layer provide a statistically more robust evaluation of the retrieval than if we relied on aircraft profiles spanning the troposphere. Finally, we evaluate the use of the OMI and MODIS cloud products for excluding cloud-contaminated observations from the comparisons.

2 Tropospheric NO_2 columns from OMI

The Ozone Monitoring Instrument (OMI) aboard the Aura satellite (launched in July 2004) is a 0.5 nm resolution UV/Visible spectrometer observing reflected sunlight from the Earth in the 270–500 nm range that can be used to derive NO_2 vertical column densities using a Differential Optical Absorption Spectroscopy (DOAS) algorithm (Levelt et al., 2006). The instrument has a 2600 km wide swath and a spatial footprint of $13 \times 24\,km^2$ at nadir. Algorithm development and validation has been carried out by both NASA-GSFC and KNMI. The two institutions have developed different operational retrieval algorithms for determining vertical column densities of NO_2, namely NASA's Standard Product and KNMI's DOMINO product. These two products use the same modified DOAS spectral analysis technique to determine NO_2 slant column densities but differ in their determination of stratospheric portion of the column and the air mass factor (AMF) – a multiplicative factor that is used to covert the slant column into a vertical column. Brief descriptions of each algorithm and their differences are included below.

2.1 NASA standard product

Details concerning the Standard Product retrieval (Level 2, Version 1.0.5, Collection 3) algorithm are provided in Bucsela et al. (2006) and Celarier et al. (2008). Briefly, the stratospheric contribution to the column is estimated by masking polluted regions and applying a zonal planetary wave smoothing. AMFs are computed as a function of viewing parameters, terrain pressure, albedo, and NO_2 profile shape and stored in a look-up table generated using the TOMRAD radiative transfer code. AMFs are calculated under both clear and cloudy conditions and a radiance-weighted sum is computed to derive the final AMF using cloud height and effective cloud fraction from the OMI O_2-O_2 cloud algorithm (Acarreta et al., 2004). Albedo is derived from observations from the Global Ozone Monitoring Experiment (GOME) satellite instrument averaged monthly to $1^\circ \times 1^\circ$ resolution until February 2009 when reflectivity was modified to OMI surface albedo climatology at $0.5^\circ \times 0.5^\circ$ (Koelemeijer et al., 2003; Kleipool et al., 2008). NO_2 profiles are from a geographically gridded set of annual mean tropospheric NO_2 profiles from the GEOS-Chem model at $2^\circ \times 2.5^\circ$ resolution.

2.2 DOMINO product

The DOMINO retrieval algorithm (Level 2, Version 1.0.2, Collection 3) is described in detail in Boersma et al. (2007). In the DOMINO product, stratospheric columns are determined by assimilating slant columns in the TM4 global chemistry and transport model. As in the Standard Product, AMF's are determined by using output from a radiative transfer model, albedo at $1^\circ \times 1^\circ$ is from Koelemeijer et al. (2003) until February 2009 when the OMI surface albedo climatology at $0.5^\circ \times 0.5^\circ$ began to be used (Kleipool et al., 2008), and cloud properties are from Acarreta et al. (2004). Daily surface pressure and NO_2 profile shape are determined by interpolating the four adjacent cells from a TM4 model output (at $3^\circ \times 2^\circ$ resolution) to the center of the OMI pixel.

2.3 The BEHR product

The Berkeley High Resolution (BEHR) retrieval uses the same method of stratospheric subtraction as that outlined for the Standard Product and AMFs are determined using the same TOMRAD-derived lookup table that depends on viewing parameters and terrain and profile information. Table 1

Table 1. Albedo, terrain pressure, and NO_2 vertical profiles in each of the three satellite column NO_2 retrievals studied here.

	NASA OMI Standard Product	Dutch OMI DOMINO Product	This Work
Albedo	* 10/04–02/09: GOME derived, $1^\circ \times 1^\circ$, Monthly; 02/09-current: OMI derived, $0.5^\circ \times 0.5^\circ$, Monthly	* 10/04–02/09: GOME derived, $1^\circ \times 1^\circ$, Monthly; 02/09-current: OMI derived, $0.5^\circ \times 0.5^\circ$, Monthly	MODIS MCD43C3, $0.05^\circ \times 0.05^\circ$, 16 day average every 8 days (averaged to OMI pixel)
Terrain Pressure	SDP Toolkit 90 arcsec DEM map (pressure @ center of OMI footprint)	TM4 model, $3^\circ \times 2^\circ$ resolution, interpolate four adjacent cells to the center of the OMI pixel	GLOBE 1 km × 1 km topographical database (averaged to OMI pixel)
NO_2 Profile	GEOS-Chem $2^\circ \times 2.5^\circ$, Annually	TM4 model, $3^\circ \times 2^\circ$ resolution, Daily, interpolate four adjacent cells to the center of the OMI pixel	WRF-Chem 4 km × 4 km, Monthly (averaged to OMI pixel)

* Note: As of early 2009, the product uses OMI reflectivity at $0.5^\circ \times 0.5^\circ$ resolution, however, the switch has not yet been retroactive and early data still uses the GOME $1^\circ \times 1^\circ$ resolution reflectivity product.

compares terrain and profile parameters implemented in the Standard Product, the DOMINO product, and our BEHR retrieval. We recalculate AMFs using the GLOBE (Global Land One-kilometer Base Elevation) $1 \times 1\,km^2$ topographical database, MODIS (Moderate Resolution Imaging Spectroradiometer) $0.05^\circ \times 0.05^\circ$ 16-day average albedo (produced every 8 days), and WRF-Chem monthly-averaged, $4 \times 4\,km^2$ simulated NO_2 profiles. The following sections describe the estimated uncertainties associated with each parameter in the two publicly available retrievals and the differences we observe between our improved NO_2 product and the operational retrievals.

3 Evaluation of the BEHR retrieval

In this section we describe each of the new datasets implemented into the BEHR retrieval and then compare the product with each individual parameter implemented with the operational products.

3.1 Terrain pressure effects

Recent studies have shown that inaccurate terrain pressure can have a significant effect on the retrieved NO_2 vertical column density. A systematic topography bias in the DOMINO product of ∼80 hPa was reported by Zhou et al. (2009). They attributed the bias to the coarse resolution of the TM4 modeled terrain pressures. Hains et al. (2010) also found that terrain pressures estimated by TM4 were 72–99 hPa larger than those they estimated, inducing a 5–20 % systematic error in the retrieved NO_2 vertical column densities. The accuracy of the pressure database used in the Standard Product has not been rigorously evaluated.

Here, we use the GLOBE topographical database to estimate terrain height for OMI NO_2 retrieval (Hastings et al., 1999). We average the high resolution dataset over the area of the satellite pixel instead of using the terrain pressure at the center of the OMI pixel as in the NASA and KNMI products. Figure 1a shows a map of the difference between terrain pressures utilized in the Standard Product and those used in the BEHR retrieval for a single day, 18 June 2008. Little change is observed where the terrain is flat (e.g. California's central valley), while larger differences are observed in the mountains. Differences on the order of ±10 % are observed, with pressures from the Standard Product generally larger than those in the BEHR retrieval. A comparison with the DOMINO product (not shown) revealed similar results. This bias is in agreement with that observed for the DOMINO product by both Zhou et al. (2009) and Hains et al. (2010). Figure 1d shows the percent change in tropospheric NO_2 column as a function of the percent change in terrain pressure and Fig. 1f shows a histogram of the percent change in tropospheric NO_2 column. Differences in column are of the order ±20 %.

3.2 Albedo effects

We use a 16-day average albedo product, retrieved every 8 days, from the MODIS instrument aboard the Aqua satellite (MCD43C3; http://modis.gsfc.nasa.gov/) which provides a much-improved spatial ($0.05^\circ \times 0.05^\circ$; $\sim 5 \times 5\,km^2$) and temporal resolution when compared with the monthly averaged $1^\circ \times 1^\circ$ GOME product and $0.5^\circ \times 0.5^\circ$ OMI product currently employed in the operational retrievals. Since both OMI and MODIS instruments are part of the A-train constellation and observe the earth within 15 minutes of one another, terrain reflectivity is captured at similar viewing and solar geometries as OMI observations of NO_2. Changes in reflectivity are better captured by the enhanced temporal and spatial resolution of MODIS, providing better representation of reflectivity over the OMI footprint. The two instruments

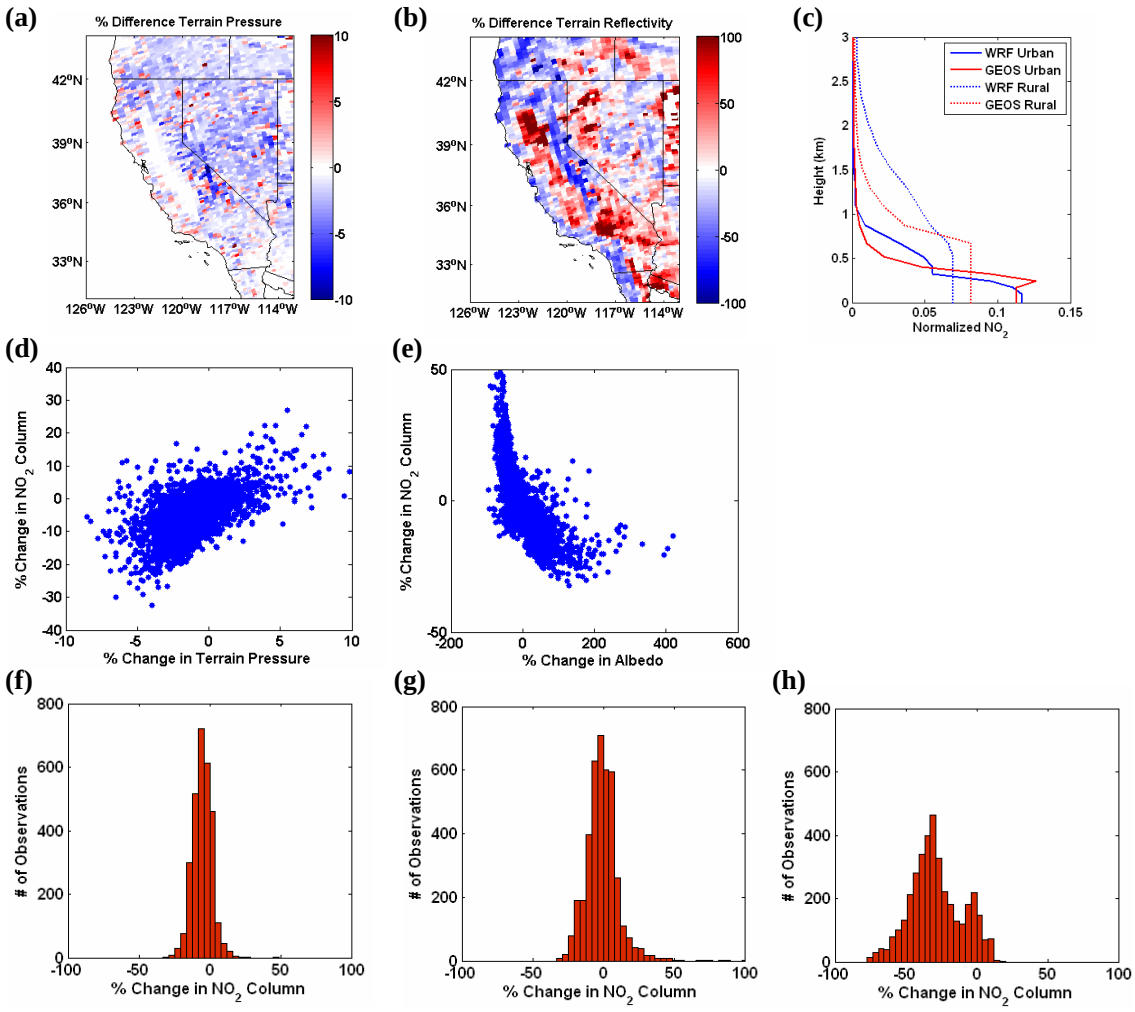

Fig. 1. Retrieval inputs from the BEHR retrieval are compared with those from the Standard Product. Maps of the percent change in **(a)** terrain pressure and **(b)** and terrain reflectivity for 18 June 2008. **(c)** Profile shapes from GEOS-Chem and WRF-Chem for single points over urban and rural regions in California. The percent change in NO_2 column versus the percent change in **(d)** terrain pressure and **(e)** albedo. Histograms of the percent change in NO_2 column due to changes in **(f)** terrain pressure, **(g)** albedo, and **(h)** NO_2 profile shape.

have different spectral bandwidths (OMI at 405–465 nm and MODIS at 459–479 nm), however, the error associated with this difference is expected to be much smaller than the error induced by the coarse spatial resolution of the current albedo products. We note that the MODIS albedo product does not provide information over the ocean so all comparisons here are for observations over land.

Figure 1b shows a map of the difference between the albedo products used in the Standard and BEHR retrievals for 18 June 2008. Differences exceeding ±100 % are observed. The percent change in tropospheric column NO_2 between the Standard Product and the BEHR NO_2 product versus the percent change in the albedo used in the two products is shown in Fig. 1e. Differences in tropospheric column NO_2 due to the effects of albedo are as large as ±40 % (Fig. 1g).

To demonstrate the effects of albedo on the tropospheric NO_2 product in further detail, we evaluate a small region in northwestern Nevada where reflectivity is highly variable. Figure 2a shows an image of a salt flat as observed by MODIS. This region is isolated with no significant sources of NO_x. A summertime average (June–August 2008) of the OMI Standard Product tropospheric NO_2 column, however, shows enhanced NO_2 in a spatial pattern resembling the reflectivity over the region (Fig. 2e). This feature arises because the coarse albedo used in the operational products ($1° \times 1°$) is unable to capture contrasts at this spatial scale (Fig. 2b). Coarse averaging of the reflectivity with less reflective, surrounding terrain yields a lower albedo. As surface albedo decreases, the AMF decreases, and the retrieved NO_2 is enhanced (Fig. 2e). By employing a more resolved albedo in the BEHR product (Fig. 2d), however, this false

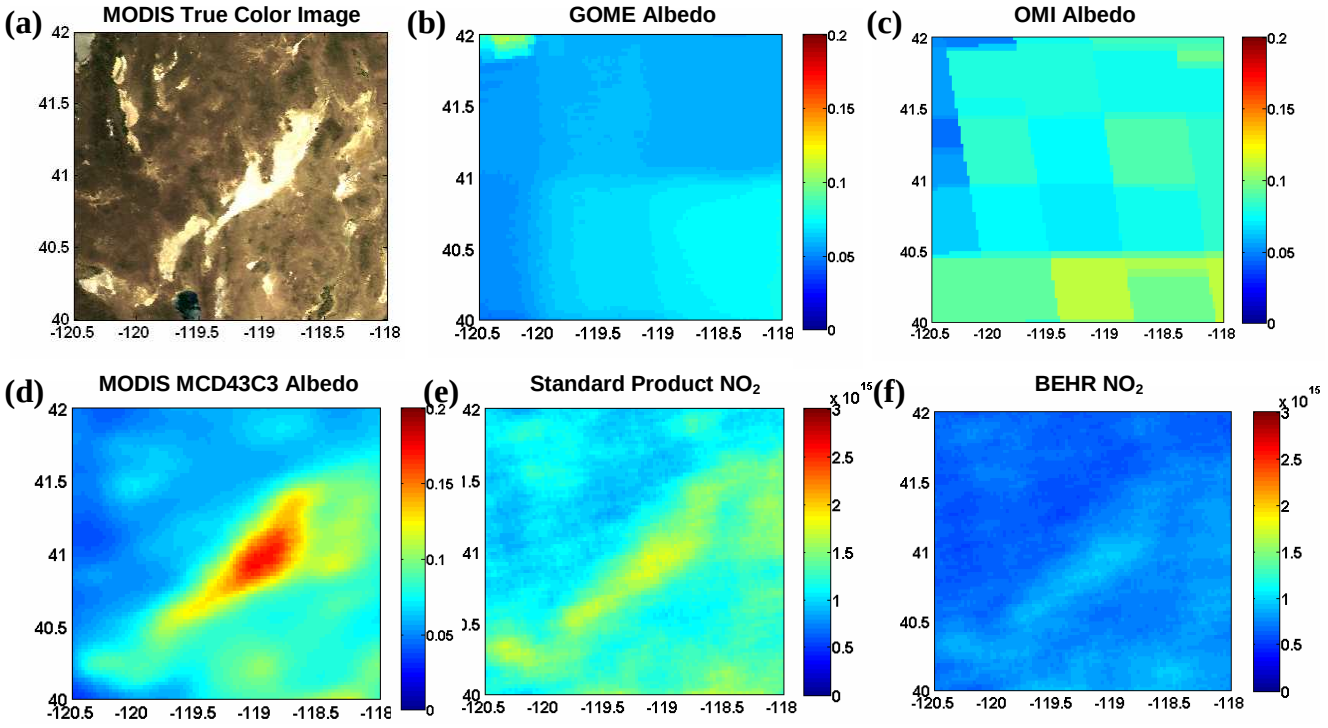

Fig. 2. **(a)** MODIS true color image of a salt flat in north western Nevada on 18 June 2008. Albedo used in **(b)** the operational retrievals for October 2004–February 2009 (GOME climatology, monthly at $1^\circ \times 1^\circ$), **(c)** the operational retrievals for February 2009 – today (OMI climatology, monthly at $0.5^\circ \times 0.5^\circ$), and **(d)** the BEHR retrieval (MODIS MCD43C3, 16 day average every 8 days, at $0.05^\circ \times 0.05^\circ$) for 18 June 2008. Average OMI tropospheric NO_2 column from **(e)** the Standard Product and **(f)** the BEHR retrieval for June-August 2008.

signal is almost fully diminished (Fig. 2f), a reduction of approximately 33 % relative to the operational products. We find that 67 % of the decrease is due to the improved albedo while the remainder is from using our improved terrain pressures and WRF-Chem profiles. The remaining enhancement may be due to the presence of clouds or aerosols, or to errors in the MODIS albedo.

3.3 NO_2 profile shape effects

The sensitivity of OMI to NO_2 is inversely related to altitude. As a result, the observed tropospheric NO_2 column depends on the NO_2 profile shape. When NO_2 is highly concentrated close to the surface, the AMF is smaller and the NO_2 column is enhanced. The operational DOMINO and Standard products currently use daily TM4 modeled profiles and annually averaged profiles from GEOS-Chem, respectively (Table 1). The profiles provided by both models are at a much coarser spatial resolution that the OMI observation (WRF-Chem: $2^\circ \times 2.5^\circ$; TM4: $3^\circ \times 2^\circ$). Consequently, an average semi-polluted profile is applied over the large grid cell that contains both urban and rural locations, poorly representing the actual NO_2 profile over both areas and resulting in an underestimation of the NO_2 column in the urban region and an overestimate in the rural region. In addition to these biases due to resolution, Lamsal et al. (2010) found that the OMI Standard Product is biased high in summer, which they attribute to the lack of seasonality in the Standard Product NO_2 profiles.

We use monthly averaged NO_2 profiles from a WRF-Chem simulation at 4km resolution. Briefly, WRF-Chem is a state-of-the-art, multi-scale regional 3-D air quality chemical transport model (Grell et al., 2005). The domain covers $2304 \times 2304\,km^2$ centered on the state of California (30–50 N, -124W$--100$ W). Emissions are the National Emission Inventory (NEI) 2005 on-road and off-road transportation emissions for a typical June weekday at native $4\,km \times 4\,km$ resolution. Emissions from lightning and fires are not included but are expected to have a minimal influence in the urban regions studied here. More information concerning emissions is available at: ftp://aftp.fsl.noaa.gov/divisions/taq/emissions_data_2005/Weekday_emissions/readme.txt. The model meteorology was driven by initial and boundary conditions derived from the North American Regional Reanalysis for July, 2005 (NARR-http://nomads.ncdc.noaa.gov/dods/NCEP_NARR_DAILY). We use the Regional Acid Deposition Model, version 2 chemical mechanism (Stockwell et al., 1990).

Using monthly averaged WRF-Chem profiles allows us to eliminate the seasonal bias observed in the Standard Product that results from the use of annually averaged profiles (Lamsal et al., 2010). As before, profiles are averaged over the satellite pixel area. Figure 1e shows normalized NO_2 profiles for a single point over an urban region in the Los Angeles area and over a rural region in coastal northern California from the GEOS-Chem and WRF-Chem models. A histogram showing the percent difference in tropospheric NO_2 column between the Standard Product and BEHR retrieval is shown in Fig. 1h. Implementation of WRF-Chem profiles results in a decrease in column NO_2 of 29 % on average, compared to the Standard Product. As expected, decreases are observed over remote areas while enhancements are observed over highly polluted, urban regions.

3.4 Spatial resolution and cloud effects

Retrieval of boundary layer NO_2 from space-based observations is highly sensitive to cloud cover. As a result, previous studies have used cloud filters in order to exclude data that has a higher uncertainty due to cloud contamination. These filters have generally been set to exclude data with a cloud fraction greater than 0.2–0.3 or data with a cloud radiance fraction greater than 0.5–0.7 according to cloud information from the OMI O_2-O_2 cloud product.

The OMI O_2-O_2 cloud algorithm relies on the 477 nm absorption band of the O_2-O_2 collision complex to estimate cloud height and fraction. Shielding of the O_2-O_2 column by the presence of clouds allows determination of cloud parameters when radiance observations are coupled with viewing geometry and terrain information and processed in a radiative transfer model. As in the OMI NO_2 products, the OMI cloud algorithm also relies on the coarse $1^\circ \times 1^\circ$ albedo from GOME. Consequently, over bright surfaces, the algorithm has trouble discerning whether the high reflectivity is from the ground or from a cloud. The algorithm thereby has a tendency to mistakenly identify clear-sky, highly reflective regions as cloudy. This error results primarily from a dependence on the coarsely-resolved reflectivity and terrain pressure currently used in the cloud algorithm. While use of the OMI cloud product has the advantage of providing cloud information that is perfectly co-located with NO_2 observations, eliminating concerns of instrumental biases, cloud retrieval from OMI is subject to large uncertainty due to the poorly resolved terrain parameters currently used in the product.

To illustrate this, Fig. 3a, b show maps of OMI O_2-O_2 derived cloud fraction and MODIS MCD43C3 albedo over California for 18 June 2008. The OMI product shows high cloud fractions over regions of high reflectivity in north western Utah, north western Nevada, and the California-Mexico border, east of San Diego. In contrast, no clouds are observed in these regions using the MODIS MYD06 cloud product (Fig. 3c). In light of this issue with the OMI O_2-O_2 cloud product, we perform our validation analyses by filtering according to both OMI and MODIS cloud fractions (averaged to the OMI pixel size) as a test of the impact of the two cloud products on the comparisons.

3.5 BEHR OMI NO_2

Figure 4 compares average tropospheric NO_2 columns for June 2008 from the Standard Product (Fig. 4a) and the BEHR retrieval (Fig. 4b) with all new terrain and profile parameters implemented. The percent difference in retrieved tropospheric NO_2 column is shown in Fig. 4c. NO_2 columns determined using the BEHR retrieval are, on average, 31 % lower than those observed using the Standard Product. Exceptions to this decrease occur in urban regions where we observe an average increase of 8 % that is primarily due to improved NO_2 profiles, and to a lesser extent, improved albedo.

4 Validation of the BEHR retrieval

In order to validate the accuracy of the BEHR product, we use in situ boundary layer measurements of NO_2 collected during the California portion of the Arctic Research of the Composition of the Troposphere from Aircraft and Satellites (ARCTAS-CA) field campaign. The ARCTAS-CA campaign was carried out in order to improve our understanding of emissions, chemical dynamics and air quality over the state of California (Jacob et al., 2010). Aircraft observations were collected on 18, 20, 22, and 24 June 2008 and a substantial fraction of the measurements were collected within the planetary boundary layer. Previous validation efforts have extrapolated columns from surface networks, which are numerous but influenced by local sources, or full aircraft spirals which are sparse (Martin et al., 2006; Bucsela et al., 2008; Lamsal et al., 2008; Boersma et al., 2009; Hains et al., 2010). Boundary layer observations, however, have the advantage of being removed from the direct influence of sources making them more representative of the tropospheric column. Further, given that individual boundary layer aircraft observations largely outnumber full vertical profile observations, their use as a validation tool greatly enhances the robustness of validation analyses.

4.1 Inferred columns from boundary layer observations

The in situ observations of NO_2 studied here were collected throughout the troposphere using the UC-Berkeley Laser-Induced Fluorescence (LIF) instrument aboard NASA's DC-8 aircraft. Details concerning the instrument are provided in Thornton et al. (2000) and Cleary et al. (2002). Briefly, the LIF system employs a Q-switched, frequency-doubled Nd^{3+}:YAG laser to pump a tunable dye laser. Following cooling of the sample via supersonic expansion to increase the population of NO_2 molecules at a target rotational level, the dye laser is held at the peak of the strong resonant for 9 s and then at an offline position in the continuum absorption

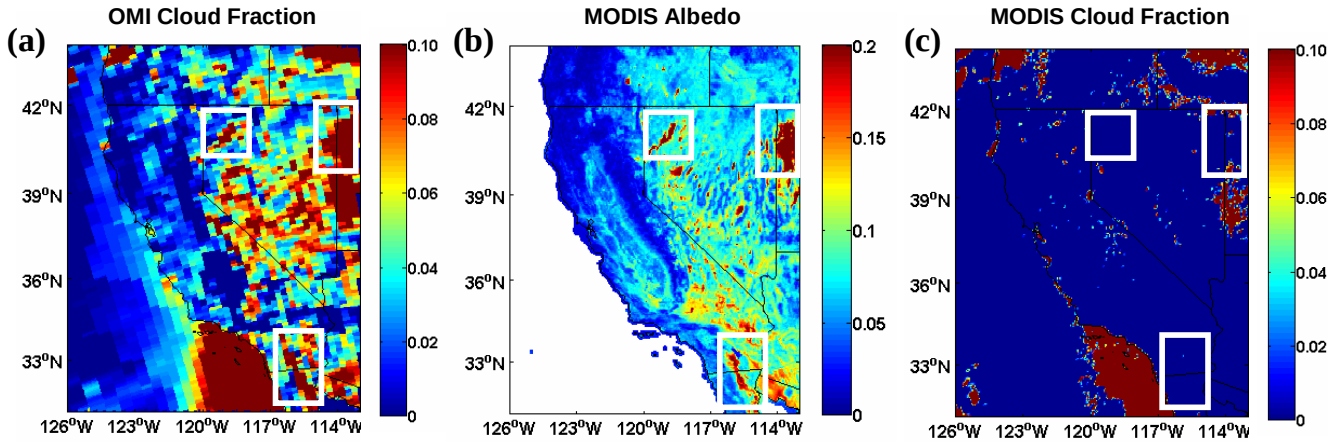

Fig. 3. Maps of California showing **(a)** OMI O_2-O_2 derived cloud fractions, **(b)** MODIS MCD43C3 albedo, and **(c)** MODIS MYD06 cloud fraction for 18 June 2008. White boxes show regions where OMI and MODIS cloud fractions do not agree due to albedo effects.

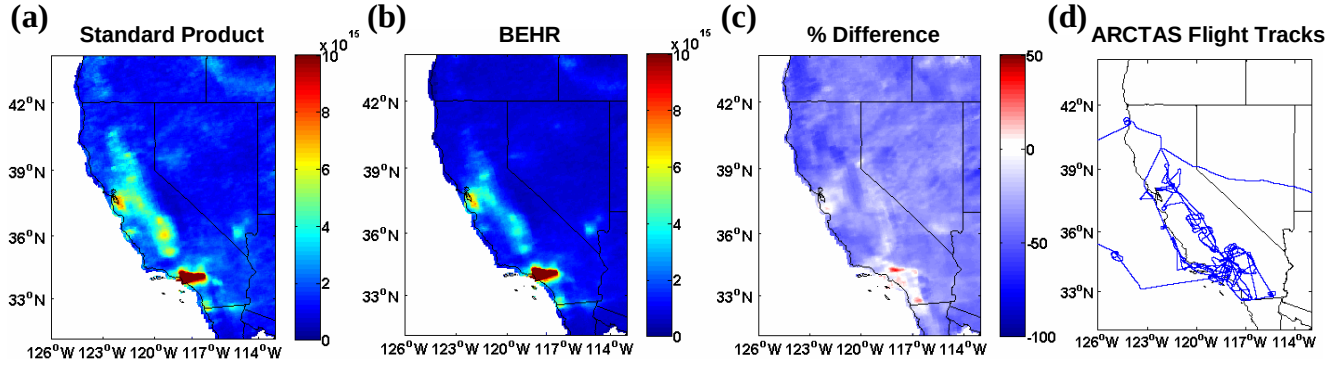

Fig. 4. Average tropospheric NO_2 column for June 2008 from **(a)** the Standard Product and **(b)** the BEHR product, and **(a)** the percent difference between the two products. **(a)** Flight tracks during the ARCTAS-CA campaign, 18-24 June 2008.

for 3 s. Fluorescence is detected at 4 Hz by a photomultiplier tube. NO_2 mixing ratio is proportional to the ratio of the peak to the background. A map showing flight tracks where in situ aircraft measurements took place during ARCTAS-CA is shown in Fig. 4d.

We estimate NO_2 vertical column densities from boundary layer aircraft observations for comparison with satellite-observed NO_2 columns by first co-locating aircraft segments that coincide with individual satellite observations (Fig. 5a). We require that each aircraft segment consist of at least 20 s of measurements that were collected within the boundary layer and within the spatial extent of an OMI pixel after discarding outliers. Outliers are defined as values that are more than two standard deviations away from the mean value for the set of measurements. An aircraft segment consists of measurements gathered between 12:00 p.m. and 03:00 p.m. local time, coinciding with the 01:45 p.m. OMI overpass time.

The boundary layer height for each aircraft observation is defined by identifying sharp gradients in aircraft measured NO_2 concentration, water vapor, and potential temperature with altitude to determine boundary layer entrance and exit points (Fig. 5b). We assume that the boundary layer height varies linearly between each entrance into and exit from the boundary layer. Observations gathered during ARCTAS-CA show small variability in NO_2 throughout the free troposphere and a mean free tropospheric concentration of roughly 40 ppt. We assume a constant 40 ppt NO_2 mixing ratio above the boundary layer for the free-tropospheric portion of the column. We further assume that the boundary layer is well-mixed in order to infer the boundary layer portion of the column from aircraft observations. This assumption generally agrees well with GEOS-Chem and WRF-Chem simulations as well as the in situ aircraft observations examined here (e.g. Fig. 1c). Further, in the analyses that follow, similar variance between aircraft and satellite observations is observed if an exponential profile is assumed. The segment of aircraft measurements associated with a single satellite pixel are averaged and integrated from the terrain height to the height of the boundary layer in order to determine the

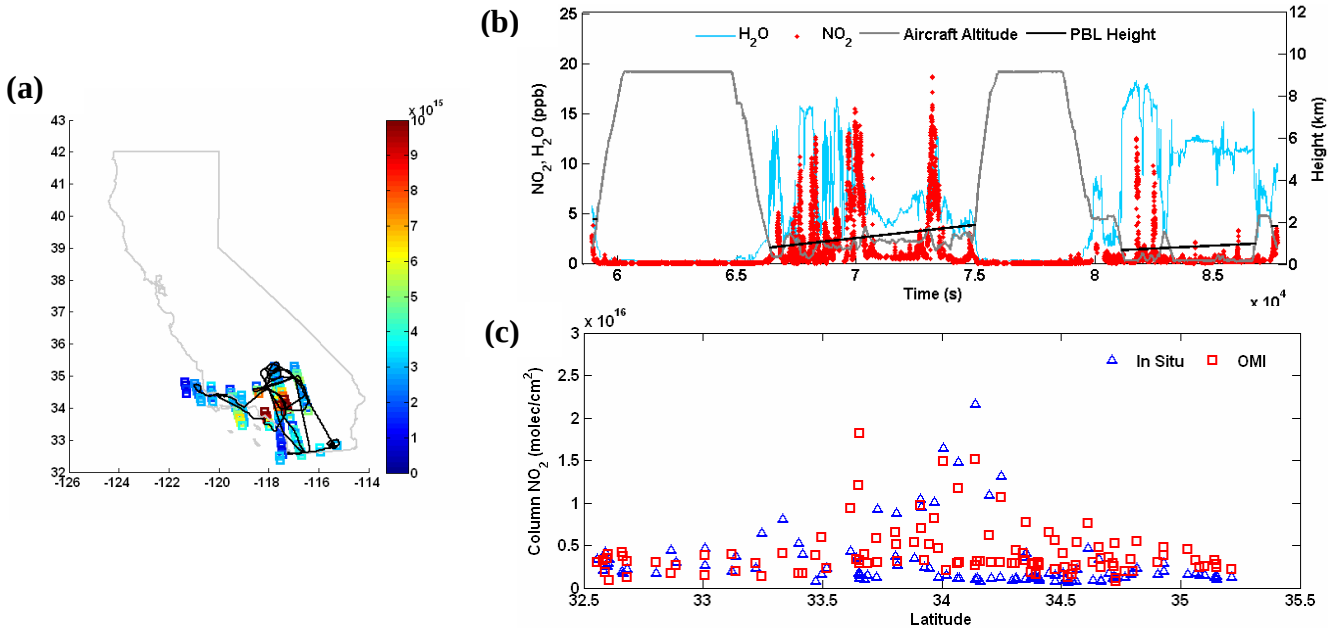

Fig. 5. (a) The black line shows the flight path over CA of the DC-8 aircraft on 24 June 2008. Colored squares show the column concentration and location of the center of coincident OMI pixels. **(b)** Aircraft altitude, H_2O vapor concentration, NO_2 concentration, and inferred boundary layer height versus time for the flight on 24 June. **(c)** In situ derived and OMI Standard Product columns collected on 24 June.

vertical column density. A preliminary comparison between in situ-derived and satellite-observed vertical column densities is shown in Fig. 5c.

In the analyses that follow, we exclude comparisons for which OMI pixels were flagged during the retrieval process as well as pixels with an OMI-derived cloud fraction greater than 20 %. A total of sixty-eight comparisons remain following the filtering processes.

4.2 Satellite observations versus inferred columns

Figures 6a, b compare the in situ-derived tropospheric column NO_2 from aircraft observations with satellite-observed column NO_2 derived using the Standard Product and DOMINO product algorithms. There is good agreement between in situ and remote-sensed observations, with correlation coefficients of $R^2 = 0.72$ and $R^2 = 0.65$ for the Standard Product and DOMINO product, respectively. Slopes associated with the fits suggest there is no bias in the Standard Product for this time of year but that the DOMINO product is biased high relative to the in situ observations. A similar bias in the DOMINO product was found by Bucsela et al. (2008) using observations from the PAVE, INTEX-A, and INTEX-B aircraft validation campaigns.

Figure 6c compares tropospheric NO_2 columns derived from in situ aircraft observations with the columns from the BEHR product. A slope of 0.96 suggests that there is no significant bias between inferred NO_2 columns and the BEHR product. We further observe a dramatically improved correlation between BEHR columns and the in situ derived observations ($R^2 = 0.83$) compared to the Standard and DOMINO products. This suggests that a large contribution to the uncertainty in OMI observations arises from biases resulting from unresolved terrain and profile databases that are currently implemented in the operational retrievals.

4.3 OMI versus MODIS cloud products

Table 2 summarizes our results for the BEHR product when employing various cloud-filters. For the MODIS cloud filtering case, the cloud fraction derived by MODIS and averaged over the OMI satellite pixel is implemented in the AMF calculation to determine NO_2 columns (while the standard OMI cloud product is used for the SP and DOMINO cloud-filtering cases). We observe a similar correlation between aircraft and remote-sensing observations when stricter OMI O_2-O_2 cloud restrictions are imposed ranging from 20 % to 5 % cloud fraction. A decrease in the correlation is observed, however, when we impose a 0 % cloud threshold due to a substantial reduction in data points at this threshold for evaluation. When we retrieve OMI NO_2 using MODIS cloud fractions and set a 0 % MODIS cloud threshold, however, we retain a substantial number of data points and observe a much higher correlation than all other thresholds tested here. As discussed in Sect. 3.4, the poor correlation between aircraft observations and the BEHR product derived using the standard OMI cloud information is expected to result from artifacts in the OMI cloud algorithm related to the coarse terrain reflectivity used in the product.

Table 2. The number of data points available, equation for best fit line, and correlation coefficient when OMI NO_2 derived using the BEHR product is filtered according to different cloud information.

Cloud Product	Cloud Fraction	# of Data Points	Best Fit Line	R^2
OMI	20 %	68	$y = 0.96x - 5.01 \times 10^{14}$	0.83
	10 %	64	$y = 0.95x - 4.38 \times 10^{14}$	0.83
	5 %	42	$y = 1.00x - 4.45 \times 10^{14}$	0.82
	0 %	11	$y = 1.56x - 5.13 \times 10^{13}$	0.58
MODIS	0 %	45	$y = 1.03x - 1.39 \times 10^{14}$	0.91

Table 3. Equation for the best fit line and correlation coefficient for satellite columns versus in situ columns when the OMI cloud fraction and MODIS cloud fraction thresholds are used.

	OMI cloud fraction <20 %	MODIS cloud fraction = 0 %
Standard Product	$y = 0.99x + 4.51 \times 10^{14}$ $R^2 = 0.72$	$y = 1.04x + 5.45 \times 10^{14}$ $R^2 = 0.86$
DOMINO	$y = 1.78x - 1.31 \times 10^{15}$ $R^2 = 0.65$	$y = 1.70x - 4.67 \times 10^{13}$ $R^2 = 0.83$
BEHR	$y = 0.96x - 5.01 \times 10^{14}$ $R^2 = 0.83$	$y = 1.03x - 1.39 \times 10^{14}$ $R^2 = 0.91$

In Table 3 we compare how the relationship between inferred columns and satellite NO_2 changes for each NO_2 product when we impose a MODIS cloud fraction threshold of 0 % (Fig. 6; dark crosses) as opposed to the OMI O_2-O_2 20 % cloud fraction threshold (Fig. 6; all crosses). For all three NO_2 products, the fits to observations with a MODIS cloud fraction of 0 % have similar slopes as the fits to observations with an OMI cloud fraction less than 20 %. We observe improved correlations when using the MODIS cloud threshold for all three products (Standard Product: $R^2 = 0.86$; DOMINO: $R^2 = 0.83$; BEHR: $R^2 = 0.91$).

4.4 Boundary layer versus complete spiral analyses

In Fig. 6 we compare the relationship between inferred columns from ARCTAS-CA in situ observations and the BEHR tropospheric column NO_2 using our boundary layer validation method (crosses) and the traditional validation method requiring measurements from full aircraft spirals spanning the troposphere as described in Hains et al. (2010; triangles). Briefly, the Hains et al. method requires that part of the aircraft segment was collected between 500 m and 2 km above the land surface, that the aircraft observations were collected within 3 h of the OMI overpass, and that the cloud radiance fraction (as observed by OMI) was less than 0.5. Aircraft observations are extrapolated to an assumed tropopause height of 12 km and the highest (lowest) 10 altitude observations are used to extrapolate to the top (bottom) of the column.

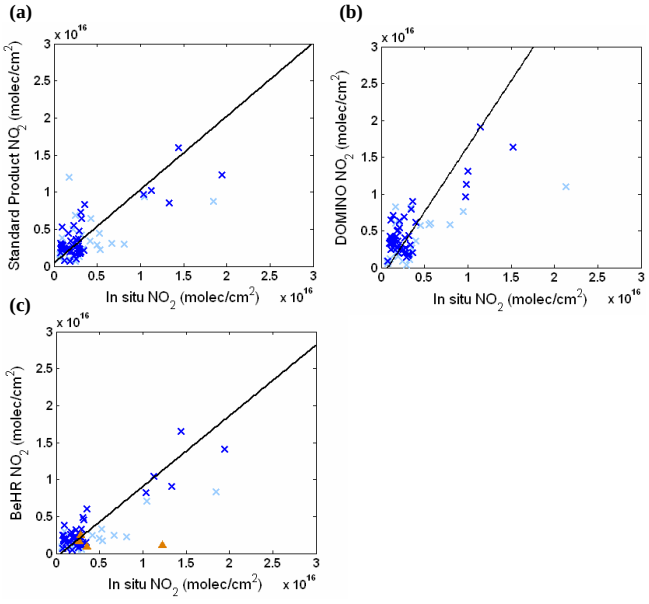

Fig. 6. OMI tropospheric column from **(a)** the Standard Product, **(b)** the DOMINO product, and **(c)** BEHR product versus coincident aircraft-derived column NO_2. Observations are over land only. All observations correspond to an OMI cloud fraction of less than 20 %. Dark blue points show where MODIS cloud fraction is 0 %. The black line shows the fit to all data. Fits and correlations are included in Table 3. Orange triangles in **(c)** show the comparison of the BEHR retrieval and in-situ derived columns determined using the full vertical spiral method in Hains et al. (2010).

The boundary layer and full aircraft spiral validation methods show similar variance between in situ observations and the BEHR retrieval of OMI NO_2 suggesting that, using our boundary layer method, we are able to capture the variation of the tropospheric column to within the same certainty as in previous work without requiring observations that span the troposphere at every point. Requiring only points within the boundary layer is an advantage because it both increases the number of data points available for evaluation of the OMI NO_2 retrieval and increases the spatial coverage of the sampling. We find that by requiring complete spirals, only

five comparisons are possible ($R^2 = 0.26$), but by using the boundary layer method described here, we expand the number of comparisons to sixty-eight ($R^2 = 0.83$).

5 Conclusions

We have produced an improved OMI NO_2 product (BEHR) that uses much finer spatial and temporal resolution terrain and profile inputs than the operational products. With the exception of the WRF-Chem profiles, these high resolution inputs are publicly available. We use the GLOBE 1km topographical database in order to correct for terrain pressure biases. We find differences of $\pm 10\,\%$ in terrain pressure, resulting in differences of roughly $\pm 20\,\%$ in the retrieved tropospheric NO_2 column. We use MODIS albedo at higher spatial and temporal resolution than the current reflectivity products. The large spatial variability in albedo observed by MODIS, not captured by the coarse operational inputs, results in tropospheric column differences up to $\pm 40\,\%$. The spatial and temporal resolution of the NO_2 profiles were also improved in the BEHR product (WRF-Chem; $4\,\text{km} \times 4\,\text{km}$; monthly) in order to account for both spatial and seasonal variation. Compared with the Standard Product, the BEHR tropospheric NO_2 product is roughly 30 % lower for relatively clean regions and 8 % higher for urban regions where anthropogenic emissions account for a majority of the observed NO_2.

We validate tropospheric NO_2 columns from the Standard, DOMINO, and the BEHR products by comparing the OMI NO_2 columns with NO_2 measurements collected during the ARCTAS-CA field campaign. While previous comparisons of this kind have required observations spanning the troposphere, we have developed a new method that converts boundary layer NO_2 concentrations to vertical column densities. Our method vastly increases the size of the validation dataset by eliminating the need for full vertical profiles for each comparison. We find excellent agreement between in situ-derived and satellite-observed NO_2 vertical column densities. We also observe largely improved agreement with the BEHR NO_2 product over the operational products. We interpret this to mean that much of the variance in current retrievals is due not to meteorological or chemical variation, but to the low spatial and temporal resolution of the geophysical assumptions used, as evidenced by the increase in the correlation coefficient, ranging from 0.65–0.72 in the operational products, to 0.83 in the BEHR retrieval. Finally, we show that MODIS cloud observations are a useful tool for filtering cloud contaminated scenes and that their use dramatically improves agreement between satellite and aircraft observations (e.g. BEHR: $R^2 = 0.91$).

Acknowledgements. The work presented here was supported by the National Aeronautics and Space Administration grant NNX08AE566 and California Air Resources Board grant 06-328. AEP would like to acknowledge funding by NASA headquarters under the NASA Earth Systems Science Fellowship Program and by NASA grant NAG5-13668. LCV would like to acknowledge funding by NASA headquarters under the NASA Earth Systems Science Fellowship Program grant NESSF09 and by NASA grant NNX08AE566. OMI data used in this effort were acquired as part of the activities of NASA's Science Mission Directorate, and are archived and distributed by the Goddard Earth Sciences (GES) Data and Information Services Center (DISC). MODIS albedo data are distributed by the Land Processes Distributed Active Archive Center (LP DAAC), located at the US Geological Survey (USGS) Earth Resources Observation and Science (EROS) Center (lpdaac.usgs.gov).

Edited by: P. Monks

References

Acarreta, J. R., De Haan, J. F., and Stammes, P.: Cloud pressure retrieval using the O_2-O_2 absorption band at 477 nm, J. Geophys. Res., 109, D05204, doi:10.1029/2003JD003915, 2004.

Beirle, S., Platt, U., Wenig, M., and Wagner, T.: NO_x production by lightning estimated with GOME, Adv. Space Res., 34(4), 793–797, doi:10.1016/j.asr.2003.07.069, 2004.

Beirle, S., Spichtinger, N., Stohl, A., Cummins, K. L., Turner, T., Boccippio, D., Cooper, O. R., Wenig, M., Grzegorski, M., Platt, U., and Wagner, T.: Estimating the NO_x produced by lightning from GOME and NLDN data: a case study in the Gulf of Mexico, Atmos. Chem. Phys., 6, 1075–1089, doi:10.5194/acp-6-1075-2006, 2006.

Beirle, S., Salzmann, M., Lawrence, M. G., and Wagner, T.: Sensitivity of satellite observations for freshly produced lightning NO_x, Atmos. Chem. Phys., 9, 1077–1094, doi:10.5194/acp-9-1077-2009, 2009.

Bertram, T. H., Heckel, A., Richter, A., Burrows, J., and Cohen, R. C.: Satellite measurements of daily variations in soil NO_x emissions, Geophys. Res. Lett., 32, L24812, doi:10.1029/2005GL024640, 2005.

Boersma, K. F., Eskes, H. J., Meijer, E. W., and Kelder, H. M.: Estimates of lightning NO_x production from GOME satellite observations, Atmos. Chem. Phys., 5, 2311–2331, doi:10.5194/acp-5-2311-2005, 2005.

Boersma, K. F., Eskes, H. J., Veefkind, J. P., Brinksma, E. J., van der A, R. J., Sneep, M., van den Oord, G. H. J., Levelt, P. F., Stammes, P., Gleason, J. F., and Bucsela, E. J.: Near-real time retrieval of tropospheric NO_2 from OMI, Atmos. Chem. Phys., 7, 2103–2118, doi:10.5194/acp-7-2103-2007, 2007.

Boersma, K. F., Jacob, D. J., Trainic, M., Rudich, Y., DeSmedt, I., Dirksen, R., and Eskes, H. J.: Validation of urban NO_2 concentrations and their diurnal and seasonal variations observed from the SCIAMACHY and OMI sensors using in situ surface measurements in Israeli cities, Atmos. Chem. Phys., 9, 3867–3879, doi:10.5194/acp-9-3867-2009, 2009.

Bucsela, E. J., Celarier, E. A., Wenig, M. O., Gleason, J. F., Veefkind, J. P., Boersma, K. F., and Brinksma, E. J.: Algorithm

for NO_2 vertical column retrieval from the ozone monitoring instrument, IEEE T. Geosci. Remote, 44(5), 1245–1258, 2006.

Bucsela, E. J., Perring, A. E., Cohen, R. C., Boersma, K. F., Celarier, E. A., Gleason, J. F., Wenig, M. O., Bertram, T. H., Wooldridge, P. J., Dirksen, R., and Veefkind, J. P.: Comparison of tropospheric NO_2 from in situ aircraft measurements with near-real-time and standard product data from OMI, J. Geophys. Res., 113, D16S31, doi:10.1029/2007JD008838, 2008.

Bucsela, E. J., Pickering, K. E., Huntemann, T. L., Cohen, R. C., Perring, A. E., Gleason, J. F., Blakeslee, R. J., Albrecht, R. I., Holzworth, R., Cipriani, J. P., Navano, D. V., Segura, I. M., Hernandez, A. P., and Laporte-Molina, S.: Lightning-generated NO_x seen by OMI during NASA's TC4 experiment, J. Geophys. Res., 115, D00J10, doi:10.1029/2009JD013118, 2010.

Celarier, E. A., Brinksma, E. J., Gleason, J. F., Veefkind, J. P., Cede, A., Herman, J. R., Ionov, D., Goutail, F., Pommereau, J. P., Lambert, J. C., van Roozendael, M., Pinardi, G., Wittrock, F., Schonhardt, A., Richter, A., Ibrahim, O. W., Wagner, T., Bojkov, B., Mount, G., Spinei, E., Chen, C. M., Pongetti, T. J., Sander, S. P., Bucsela, E. J., Wenig, M. O., Swart, D. P. J., Volten, H., Kroon, M., and Levelt, P. F.: Validation of ozone monitoring instrument nitrogen dioxide columns, J. Geophys. Res., 113, D15S15, doi:10.1029/2007JD008908, 2008.

Cleary, P. A., Wooldridge, P. J., and Cohen, R. C.: Laser-induced fluorescence detection of atmospheric NO_2 using a commercial diode laser and a supersonic expansion, Appl. Optics, 41(33), 6950–6956, 2002.

Franke, K., Richter, A., Bovensmann, H., Eyring, V., Jöckel, P., Hoor, P., and Burrows, J. P.: Ship emitted NO_2 in the Indian Ocean: comparison of model results with satellite data, Atmos. Chem. Phys., 9, 7289–7301, doi:10.5194/acp-9-7289-2009, 2009.

Grell, G. A., Peckham, S. E., Schmitz, S. A., McKeen, A., Frost, G., Skamarock, W. C., and Eder, B.: Fully coupled online chemistry within the WRF model, Atmos. Environ., 39, 6957–6975, 2005.

Hains, J. C., Boersma, K. F., Kroon, M., Dirksen, R. J., Cohen, R. C., Perring, A. E., Bucsela, E., Volten, H., Swart, D. P. J., Richter, A., Wittrock, F., Shoenhardt, A., Wagner, T., Ibrahim, O. W., Van Roozendael, M., Pinardi, G., Gleason, J. F., Veefkind, J. P., and Levelt, P.: Testing and improving OMI DOMINO tropospheric NO_2 using observations from the DANDELIONS and INTEX-B validation campaigns, J. Geophys. Res., 115, D05301, doi:10.1029/2009JD012399, 2010.

Hastings, D. A., Dunbar, P. K., Elphingstone, G. M., Bootz, M., Murakami, H., Maruyama, H., Masaharu, H., Holland, P., Payne, J., Bryant, N. A., Logan, T. L., Mullter, J. P., Schreier, G., and MacDonald, J. S.: The Global Land One-kilometer Base Elevation (GLOBE) digital elevation model, Ver 1.0. eds. 1999. National Oceanic and Atmospheric Administration, National Geophysical Data Center, 325 Broadway, Boulder, Colorado 80305-3328, USA Digital data base on the World Wide Web, available at: http://www.ngdc.noaa.gov/mgg/topo/globe.html and CD-ROMs, 1999.

Heckel, A., Kim, S.-W., Frost, G. J., Richter, A., Trainer, M., and Burrows, J. P.: Influence of under-sampled a priori data on tropospheric NO_2 satellite retrievals, Atmos. Meas. Tech. Discuss., 4, 1893–1934, doi:10.5194/amtd-4-1893-2011, 2011.

Hudman, R. C., Russell, A. R., Valin, L. C., and Cohen, R. C.: Interannual variability in soil nitric oxide emissions over the United States as viewed from space, Atmos. Chem. Phys., 10, 9943–9952, doi:10.5194/acp-10-9943-2010, 2010.

Jacob, D. J., Crawford, J. H., Maring, H., Clarke, A. D., Dibb, J. E., Emmons, L. K., Ferrare, R. A., Hostetler, C. A., Russell, P. B., Singh, H. B., Thompson, A. M., Shaw, G. E., McCauley, E., Pederson, J. R., and Fisher, J. A.: The Arctic Research of the Composition of the Troposphere from Aircraft and Satellites (ARCTAS) mission: design, execution, and first results, Atmos. Chem. Phys., 10, 5191–5212, doi:10.5194/acp-10-5191-2010, 2010.

Jaeglé, L., Steinberger, L., Martin, R. V., and Chance, K.: Global partitioning of NO_x sources using satellite observations: Relative roles of fossil fuel combustion, biomass burning and soil emissions, Faraday Discuss., 130, 407-423, 2005.

Kim, S.-W., Heckel, A., McKeen, S. A., Frost, G. J., Hsie, E.-Y., Trainer, M. K., Richter, A., Burrows, J. P., Peckham, S. E., and Grell, G. A.: Satellite-observed U.S. power plant NO_x emission reductions and their impact on air quality, Geophys. Res. Lett., 33, L22812, doi:10.1029/2006GL027749, 2006.

Kim, S. W., Heckel, A., Frost, G. J., Richter, A., Gleason, J., Burrows, J. P., McKeen, S., Hsie, E. Y., Granier, C., and Trainer, M.: NO_2 columns in the western United States observed from space and simulated by a regional chemistry model and their implications for NO_x emissions, J. Geophys. Res., 114, D11301, doi:10.1029/2008JD011343, 2009.

Kleipool, Q. L., Dobber, M. R., de Haan, J. F., and Levelt, P. F.: Earth surface reflectance climatology from 3 years of OMI data, J. Geophys. Res., 113, D18308, doi:10.1029/2008JD010290, 2008.

Koelemeijer, R. B. A., De Haan, J. F., and Stammes, P.: A database of spectral reflectivity in the range 335–772 nm derived from 5.5 years of GOME observations, J. Geophys. Res., 108 D2), 4070, doi:10.1029/2002JD002429, 2003.

Lamsal, L. N., Martin, R. V., van Donkelaar, A., Seinbacher, M., Celarier, E. A., Bucsela, E., Dunlea, E. J., and Pinto, J. P.: Ground-level nitrogen dioxide concentrations inferred from the satellite-borne Ozone Monitoring Instrument, J. Geophys. Res., 113, D16308, doi:10.1029/2007JD009235, 2008.

Lamsal, L. N., Martin, R. V., van Donkelaar, A., Celarier, E. A., Bucsela, E. J., Boersma, K. F., Dirksen, R., Luo, C., and Wang, Y.: Indirect validation of tropospheric nitrogen dioxide retrieved from the OMI satellite instrument: insight into the seasonal variation of nitrogen oxides at northern midlatitudes, J. Geophys. Res., 115, D05302, doi:10.1029/2009JD013351, 2010.

Levelt, P. F., Hilsenrath, E., Leppelmeier, G. W., van den Oord, G. B. J., Bhartia, P. K., Tamminen, J., de Haan, J. F., and Veefkind, J. P.: Science objectives of the Ozone Monitoring Instrument, IEEE T. Geosci. Remote, 44, 1199–1208, doi:10.1109/TGRS.2006.872336, 2006.

Lin, J. -T. and McElroy, M. B.: Detection from space of a reduction in anthropogenic emissions of nitrogen oxides during the Chinese economic downturn, Atmos. Chem. Phys. Discuss., 11, 193–223, doi:10.5194/acpd-11-193-2011, 2011.

Martin, R. V., Jacob, D. J., Chance, K., Kurosu, T. P., Palmer, P. I., and Evans, M. J.: Global inventory of nitrogen oxide emissions constrained by space-based observations of NO_2 columns. J. Geophys. Res., 108(D17), 4537, doi:10.1029/2003JD003453, 2003.

Martin, R. V., Sioris, C. E., Chance, K. V., Ryerson, T. B., Bertram, T. H., Wooldridge, P. J., Cohen, R. C., Neuman, J. A., Swan-

son, A., and Flocke, F. M. Evaluation of space-based constraints on nitrogen oxide emissions with regional aircraft measurements over and downwind of eastern North America, J. Geophys. Res., 111, D23S60, doi:10.1029/2006JD007530, 2006.

Martin, R. V., Sauvage, B., Folkins, I., Sioris, C. E., Boone, C., Bernath, P., Ziemke, J.: Space-based constraints on the production of nitric oxide by lightning, J. Geophys. Res., 112, D09309, doi:10.1029/2006JD007831, 2007.

Mebust, A. K., Russell, A. R., Hudman, R. C., Valin, L. C., and Cohen, R. C.: Characterization of wildfire NO_x emissions using MODIS fire radiative power and OMI tropospheric NO_2 columns, Atmos. Chem. Phys., 11, 5839–5851, doi:10.5194/acp-11-5839-2011, 2011.

Mijling, B., van der A, R. J., Boersma, K. F., Van Roozendael, M., De Smedt, I., and Kelder, H. M.: Reductions in NO_2 detected from space during the 2008 Beijing Olympic Games, Geophys. Res. Lett., 36, L13801, doi:10.1029/2009GL038943, 2009.

Richter, A., Burrows, J. P., Nüß, H., Granier, C, and Niemeier, U.: Increase in tropospheric nitrogen dioxide over China observed from space, Nature, 437, 129–132, doi:10.1038/nature04092, 2005.

Russell, A. R., Valin, L. C., Buscela, E. J., Wenig, M. O., and Cohen, R. C.: Space-based constraints on spatial and temporal patterns in NO_x emissions in California, 2005–2008, Environ. Sci. Technol., 44, 3607–3615, 2010.

Schaub, D., Brunner, D., Boersma, K. F., Keller, J., Folini, D., Buchmann, B., Berresheim, H., and Staehelin, J.: SCIAMACHY tropospheric NO_2 over Switzerland: estimates of NO_xlifetimes and impact of the complex Alpine topography on the retrieval, Atmos. Chem. Phys., 7, 5971–5987, doi:10.5194/acp-7-5971-2007, 2007

Stockwell, W. R., Middleton, P., Chang, J. S., and Tang, X.: The second generation regional acid deposition model chemical mechanism for regional air quality modeling, J. Geophys. Res., 95(D10), 16343–16367, doi:10.1029/JD095iD10p16343, 1990.

Thornton, J. A., Wooldridge, P. J., and Cohen, R. C.:Atmospheric NO_2: In situ laser-induced fluorescence detection at parts per trillion mixing ratios, Anal. Chem., 72, 528–539, 2000.

Valin, L. C., Russell, A. R., Bucsela, E. J., Veefkind, J. P., and Cohen, R. C.: Observation of slant column NO_2 using the super-zoom mode of AURA-OMI, Atmos. Meas. Tech. Discuss., 4, 1989-2005, doi:10.5194/amtd-4-1989-2011, 2011.

Zhou, Y., Brunner, D., Spurr, R. J. D., Boersma, K. F., Sneep, M., Popp, C., and Buchmann, B.: Accounting for surface reflectance anisotropy in satellite retrievals of tropospheric NO_2, Atmos. Meas. Tech., 3, 1185–1203, doi:10.5194/amt-3-1185-2010, 2010.